Aerosol and Air Quality Research, 18: 2253–2261, 2018

ISSN: 1680-8584 print / 2071-1409 online
doi: 10.4209/aaqr.2017.11.0452

The Controlling Factors of Photochemical Ozone Production in Seoul, South Korea

Saewung Kim[1*], Daun Jeong[1], Dianne Sanchez[1], Mark Wang[1], Roger Seco[1], Donald Blake[2], Simone Meinardi[2], Barbara Barletta[2], Stacey Hughes[2], Jinsang Jung[3], Deugsoo Kim[4], Gangwoong Lee[5], Meehye Lee[6], Joonyoung Ahn[7], Sang-Deok Lee[8], Gangnam Cho[7], Min-Young Sung[7], Yong-Hwan Lee[7], Rokjin Park[9]

[1] *Department of Earth System Science, University of California, Irvine, Irvine CA 92697, USA*
[2] *Department of Chemistry, University of California, Irvine, Irvine CA 92697, USA*
[3] *The Division of Metrology for Quality of Life, Korea Research Institute of Standards and Science, Daejeon 34113, Korea*
[4] *Department of Environmental Engineering, Kunsan National University, Kunsan 573-701, Korea*
[5] *Department of Environmental Sciences, Hankuk University of Foreign Studies, Yongin 449-791, Korea*
[6] *Department of Earth and Environmental Sciences, Korea University, Seoul 02841, Korea*
[7] *Department of Climate and Air Quality, National Institute of Environmental Research, Incheon 22689, Korea*
[8] *College of Forest and Environmental Sciences, Kangwon National University, Chuncheon 24341, Korea*
[9] *School of Earth and Environmental Sciences, Seoul National University, Seoul 08826, Korea*

ABSTRACT

We present the ambient ozone and relevant observed trace gas dataset in Seoul, South Korea, during the Megacity Air Pollution Studies (MAPS)-Seoul field campaign from May to June of 2015 (MAPS-Seoul 2015). We observed two distinctive periods, one with higher and the other with lower daytime ozone levels despite mostly clear conditions for both periods. The importance of peroxy radical contributions to excess ozone production is illustrated by the substantial differences in the Leighton constant (Φ) for the two periods. Moreover, higher levels of hydroxyl radical (OH) reactivity (s^{-1}) were observed during the high ozone episode compared to the low ozone episode by as much as ~5 s^{-1}. The contributions of nitrogen oxides (NO_x) to OH reactivity become less important than those of volatile organic compounds (VOCs) during the high ozone episode, which suggests the NO_x saturated ozone production regime. It was also notable that the biogenic VOC isoprene consistently contributed the most to OH reactivity from among the observed VOCs during the afternoon throughout the whole field campaign. Finally, we ran multiple box model scenarios to evaluate the ozone production rates of three different air mixtures: a high ozone mixture, a low ozone mixture, and a simulation of the regional air quality. The results indicate that the total OH reactivity levels and the relative contributions of VOCs to NO_x play critical roles in ozone production rates. The simulated air quality mixture results in lower OH reactivity, causing lower ozone production rates than those calculated for the high ozone mixture, which clearly indicates the need for further improvements in the regional model to accurately simulate ozone precursors in the region. The results of this study suggest that a comprehensive trace gas dataset combined with observations of the OH reactivity enables us to properly diagnose the photochemistry behind ozone pollution, leading to effective ozone abatement policies.

Keywords: Ozone; Leighton Constant; OH reactivity; Ozone production regime.

INTRODUCTION

Tropospheric ozone, a photochemical byproduct, is a reactive gas that maintains tropospheric oxidation capacity by producing $O(^1D)$ from photolysis. The minor fraction of $O(^1D)$ reacts with water vapor to produce hydroxyl radical (OH), a universal oxidant (Levy, 1971). Thus, it is vital to maintain adequate ozone levels so that it can generate OH to remove potential toxic gases such as carbon monoxide (CO) and methane (CH_4) from the troposphere. In the 1940s, excessive ozone production from pollutants such as reactive nitrogen oxide (NO_x = NO + NO_2) and volatile organic compounds was first identified at levels that could exacerbate human health and negatively impact crop yields

* Corresponding author.
Tel.: 1-949-824-4531
E-mail address: saewungk@uci.edu

(Blacet, 1952; Haagen-Smit, 1952). Among the various emission sources, automobiles with internal combustion engines were highlighted as the main cause of the ozone pollution problem. In this sense, it is not surprising that an ozone pollution outbreak was first reported in Southern California in the city of Los Angeles (Haagen-Smit, 1952).

A simplified schematic of tropospheric photochemistry is illustrated in Fig. 1. The NO and NO_2 reaction cycle can be considered a catalyst while peroxy radicals (hydrogen peroxy and organic peroxy radicals, denoted as HO_2 and RO_2, respectively) fuel the production of excess ozone since the NO_x catalytic cycle involves a reaction that destroys ozone (R1).

$$NO + O_3 \rightarrow NO_2 + O_3 \quad \text{(R1)}$$

$$NO_2 + h\nu \rightarrow NO + O \quad \text{(R2)}$$

$$O_2 + O + M \rightarrow O_3 + M \quad \text{(R3)}$$

where M is the third body such as N_2 or O_2.

$$NO + HO_2 \text{ or } RO_2 \rightarrow NO_2 + OH \text{ or } RO \quad \text{(R4)}$$

$$OH + NO_2 + M \rightarrow HNO_3 + M \quad \text{(R5)}$$

$$HO_2 + HO_2 + M \rightarrow H_2O_2 + O_2 + M \quad \text{(R6)}$$

$$HO_2 + RO_2 \rightarrow ROOH + O_2 + M \quad \text{(R7)}$$

Early studies examining relationships between NO_x and ozone in urban environments in Southern California have consistently reported that a series of reactions—R1, R2, and R3—present a null cycle. This indicates that NO oxidation is mostly followed by the reaction with ozone (R1) rather than HO_2 or RO_2 (Calvert, 1976; Ridley *et al.*, 1992). In this case, the Leighton constant (Φ) becomes a unity.

$$\Phi = \frac{J[NO_2]}{k_1[NO][O_3]} \quad \text{(E1)}$$

On the other hand, once NO oxidation by peroxy radical becomes prominent (e.g., R4), the Leighton constant becomes higher than 1. Therefore, the Leighton constant allows us to gauge a relative importance of peroxy radical chemistry in the local photochemical system, specifically in ozone production (Parrish *et al.*, 1986; Crawford *et al.*, 1996; Griffin *et al.*, 2007).

The different roles of NO_x and VOCs in ozone photochemistry causes nonlinearity in ozone formation. For example, if NO_x emissions are much greater than VOC emissions, ozone formation might not be as efficient as R5 becomes the more effective radical and NO_x sink. On the other hand, in an environment where VOC emissions are relatively higher than NO_x emissions, peroxy radicals would not be able to effectively oxidize NO, and instead react with themselves (R6 and R7). The nonlinear nature became the guiding principle in establishing an effective ozone abatement policy (Seinfeld, 1989).

In this study, we will examine an observational dataset relevant to ozone photochemistry collected in the late spring of 2015 during MAPS-2015 study in Seoul, South Korea (May 15–June 15, 2015). The analysis highlights the main causes of ozone pollution in this specific megacity environment and provides a diagnostic tool set that can be applied to other photochemical environments.

METHODS

Research Site

The research site was established at Korea Institute of Science and Technology (KIST, Latitude: 37°36′10.4544″ and longitude: 127°2′46.0284″). The research site was established on elevated ground with no direct adjacent

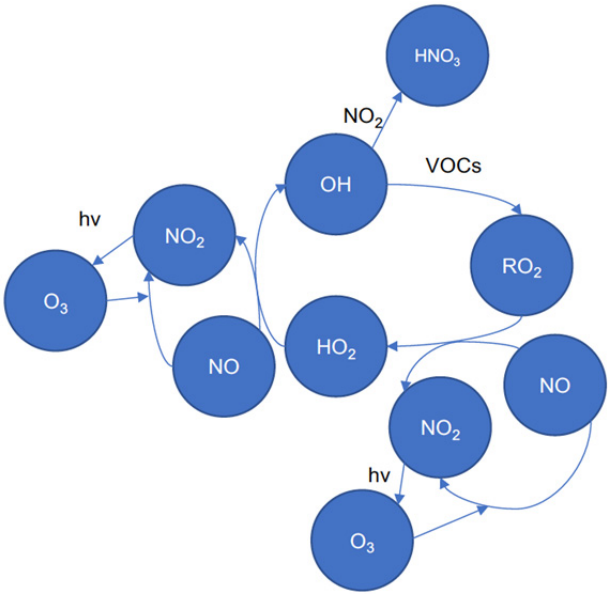

Fig. 1. Simplified schematics of tropospheric ozone photochemistry.

traffic influence. The major road is around 300 m away to the northeastern side of the site. Otherwise, the site is surrounded by a forested area, as shown in Fig. 2. The site is located ~5 km away from the city center of Seoul. The population of the Seoul Metropolitan Area (SMA) is ~25 million (2010 Government Census), which composes 48.9% of population of South Korea. The population density of the SMA is 16,700 people per 1 km^2, the densest among the cities of the countries affiliated in Organization for Economic Cooperation and Development (OECD).

Observations

The analytic methods, uncertainty and limit of detection of the species discussed in this manuscript are summarized in Table 1. Most of the observations were conducted by utilizing commercially available instruments except for the speciated VOC analysis and OH reactivity observations. The VOC analysis was conducted by canister samplings. The sampling frequency was twice per day consistently at 10 a.m. and 4 p.m. local time for a total of 24 total samples. A two-liter stainless steel canister with electropolished inner layer was utilized for sampling. Each canister was evacuated in the lab with proper pre-treatment for ambient sampling before it was sent out to the field site (Colman *et al.*, 2001). While it was sampled, extra care was taken to avoid any local contamination sources by directing inlet to upwind and carefully observing any potential contamination sources such as smoking or local traffic. The VOC analysis was conducted at the University of California, Irvine, immediately after the field campaign using a gas

Fig. 2. A satellite image (Google Earth) of SMA with a magnified view on the monitoring site.

Table 1. A summary of analytical principles and characteristics of presented observables.

Observables	Manufacturer and model number	Uncertainty	Lower limit of detection
CO	Thermo Scientific 48i TLE	10%	40 ppb
NO_x	Thermo Scientific 42i-TL with a photolysis converter	15%	50 ppt
SO_2	Thermo Scientific 43i-TLE	10%	50 ppt
Ozone	Thermo Scientific 49i	5%	< 1ppb
VOCs	Whole air sample with GC analysis (at UCI)		
OH Reactivity	Custom Built	15%	3 s^{-1}
Meteorological parameters	LSI LASTEM meteorological sensors	N/A	
J_{NO2}	Total Ultraviolet Radiometer, The Eppley Laboratory, Inc.	10%	

chromatographic system equipped with five different column-detector combinations including two flame ionization detectors, two electron capture detectors and one mass spectrometer. Details on the analytical system can be found in Colman *et al.* (2001). OH reactivity was observed using a chemical ionization mass spectrometer-comparative reactivity (CIMS-CRM) system. The analytical principle is well described in Kim *et al.* (2016) and Sanchez *et al.* (2018). Analytical methods and their characteristics applied for other presented trace gas observations in this study is summarized in Table 1.

Box Model

The Framework for 0-D Atmospheric Modeling (F0AM v 3.1) (Wolfe *et al.*, 2016) is used to evaluate ozone formation potential from different mixtures of trace gases for periods representing high (Period I; dashed red box in Fig. 3) and moderate (Period II; dashed blue box in Fig. 3) ozone episodes. The box-model framework was incorporated with the Master Chemical Mechanism (MCM v 3.3.1) that includes near-explicit VOC oxidation mechanisms (Jenkin *et al.*, 2015). The F0AM (previously named University of Washington Chemistry Model) has been used for exploring ozone and radical productions in several previous studies (Kim *et al.*, 2013; Kim *et al.*, 2015). The goal of the model analysis in this study was to mimic a chamber experiment by constraining each reaction step with field observations and investigate the production of ozone. A total of 41 VOCs, presented in Kim *et al.* (2016) and other trace gases (i.e., CO, NO, NO_2) measured at 4 p.m. local time were averaged for low and high ozone episodes during the campaign and constrained in the model. The photolysis rate constants were scaled based on measured J_{NO2}.

RESULTS AND DISCUSSION

The temporal variations of trace gases relevant to ozone photochemistry is shown in Fig. 3. As described in Kim *et al.* (2016), the regional traffic emission causes consistently high NO_x. The concentrations of most criteria pollutants are comparable to levels reported from Tokyo, Japan, and lower than levels reported from cities in China (Beijing, Tianjin, and Shanghai) (Kim *et al.*, 2016). In terms of particulate pollution, the study period is considered less polluted compared to previous years (Lee *et al.*, 2017). Nonetheless, ozone during the study period was at higher levels than what is considered healthy for children, elderly, and other susceptible individuals. The South Korean federal government has set their ozone attainment level at 60 ppb over an eight-hour average and 100 ppb for a one-hour average. In Fig. 3, the 100 ppb limit is shown by a dashed line over the ozone temporal variation. There are 7 days where the ozone concentration exceeds 100 ppb in considerable duration (e.g., more than an hour).

Fig. 4 depicts the average diurnal variations of relevant parameters during high (Period I) and moderate (Period II)

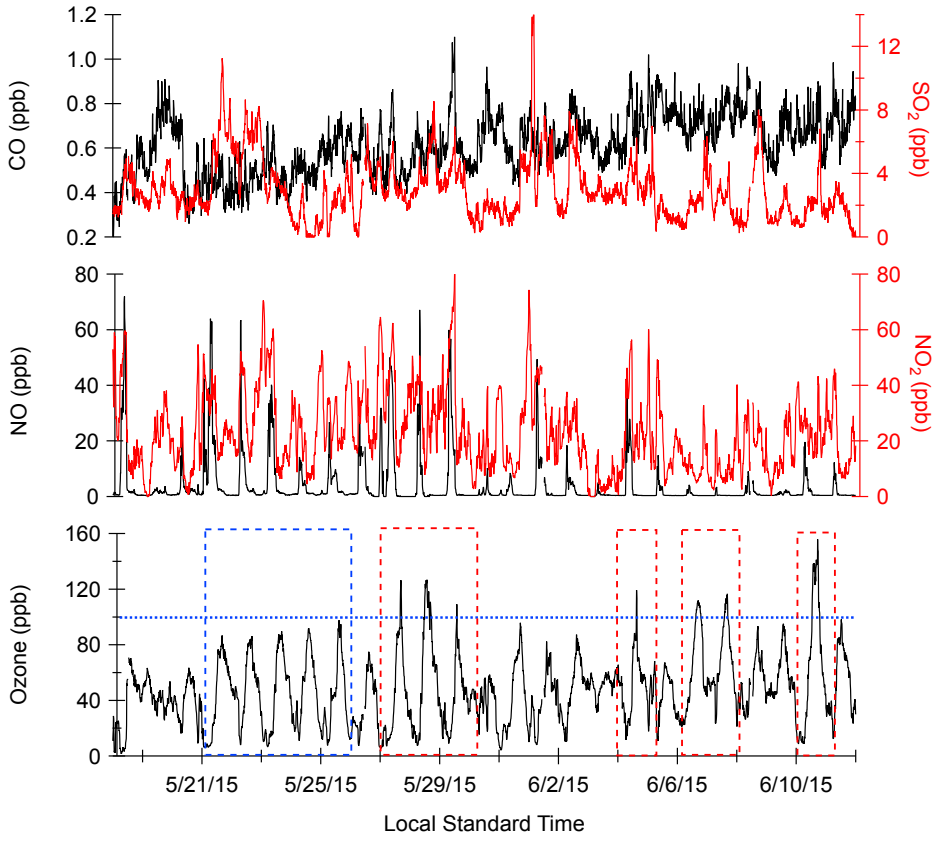

Fig. 3. The temporal variations of CO, SO_2, NO, NO_2, and ozone during the MAPS-Seoul 2015 field campaign. Two distinctive periods with high ozone (red) and low ozone (blue) are shown as the dashed boxes among the mostly clear days.

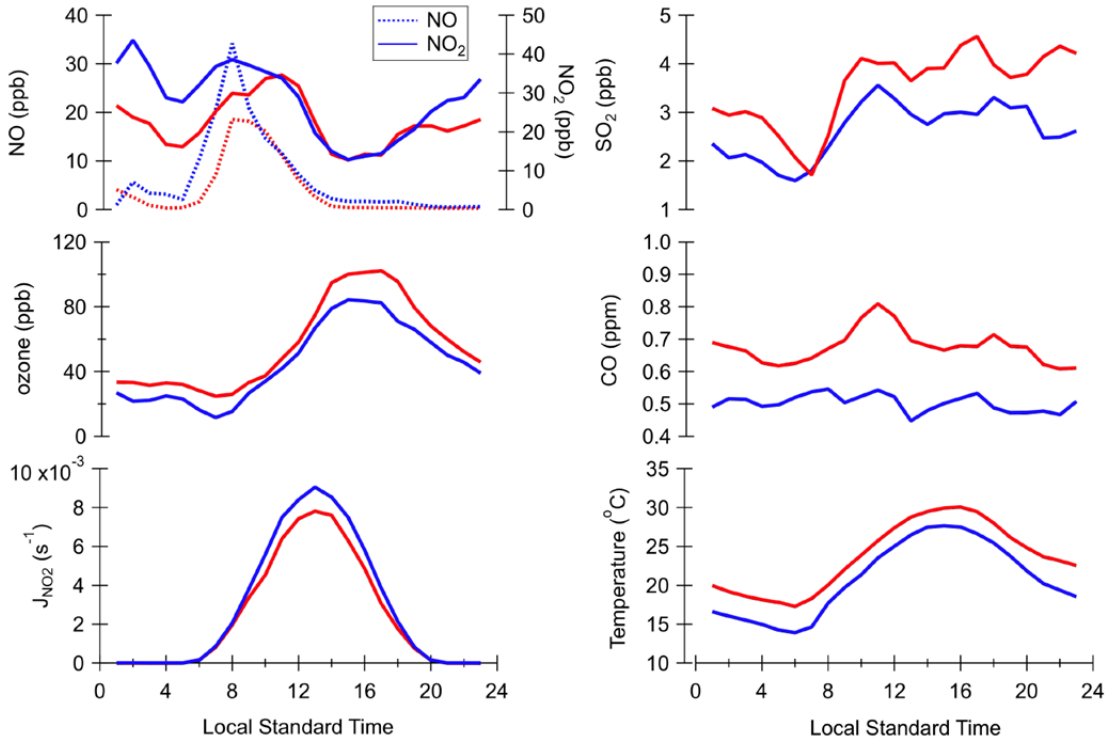

Fig. 4. The diurnal variations of trace gases for high ozone (Period I in red) and low ozone (Period II in blue) periods. The specific dates considered for statistics are shown in Fig. 1.

ozone pollution episodes. The specific dates considered for the diurnal variations are in dashed red (Period I) and blue (Period II) boxes in Fig. 3. We observed higher levels of relatively long-lived pollutants such as CO and SO_2 during Period I. The NO_x (NO and NO_2) levels do not show systematic differences during ozone's daily maximum in the afternoon. Systematically higher levels of J_{NO2} were observed during Period II, although temperature appeared consistently higher during Period I that will cause a higher rate constant for R1. In summary, it is not entirely clear whether any one parameter triggered the observed high ozone episodes as both J_{NO2} and k_1 are direct input parameters for the calculation of the Leighton constant (E1).

The temporal variations of ozone and the Leighton constant are presented in Fig. 5(a). There are significant differences in the Leighton constant between Period I and Period II. The average diurnal variations of the Leighton constant of Period I and Period II are shown in Fig. 5(b). The calculated constant is conspicuously higher during Period I, confirming the systematic differences. These differences are especially pronounced during the afternoon. Fig. 5(c) demonstrates linear correlation between the Leighton constant and ozone between 1:00 p.m. and 3:00 p.m., local time. A general tendency that higher NO_2 positively correlates with the higher Leighton constant is observed from the color-coded data point by NO_x mixing ratios in a given ozone concentration bin. Considering the nonlinear nature of ozone tropospheric photochemistry, it is difficult to attribute a single reason behind this correlation. Nonetheless, the Leighton constant tends to be higher when peroxy radials become a dominant oxidant for the NO to NO_2 conversion, leading to a net ozone production. From the OH radical recycling perspective, reactions between OH and NO_2 would act as a sink to both NO_x and HO_x. However, reactions between OH and CO or VOCs lead to OH recycling and ozone production in high NO_x environments, such as this study location (Fig. 1). Consequently, OH reactivity should also have a direct impact in the ozone production regime. Kirchner *et al.* (2001), proposed that the OH reactivity ratio of VOCs and NO_x is a better predictor of the ozone production regime (NO_x-limited or VOC limited regimes) than the concentration-based metrics. Sinha *et al.* (2012) supported this notion and proposed that OH reactivity measurements be used as a tool for assessing ozone production rates and informing ozone abatement policies.

The observed OH reactivity indicates that, on average, NO_x was the dominant contributor to the calculated OH reactivity from the trace gas observational dataset. NO_x contributed as much as 55% in the morning and 43% in the afternoon (Kim *et al.*, 2016). VOCs contributed 33% and 39% in the morning and afternoon, respectively, to the calculated OH reactivity during the study period. The biggest contributor to OH reactivity in the afternoon (47%) among the observed VOCs was isoprene, a biogenically emitted VOC (BVOC). Fig. 6 depicts the diurnal variations of observed and calculated OH reactivity from Periods I and II. The total calculated OH reactivity, including VOCs, is represented by blue star markers for each period. The markers are only presented at 4 p.m. local standard time when the VOC samplings were conducted. Although the total calculated OH reactivity accounts for the observed OH reactivity in the afternoon within the analytical

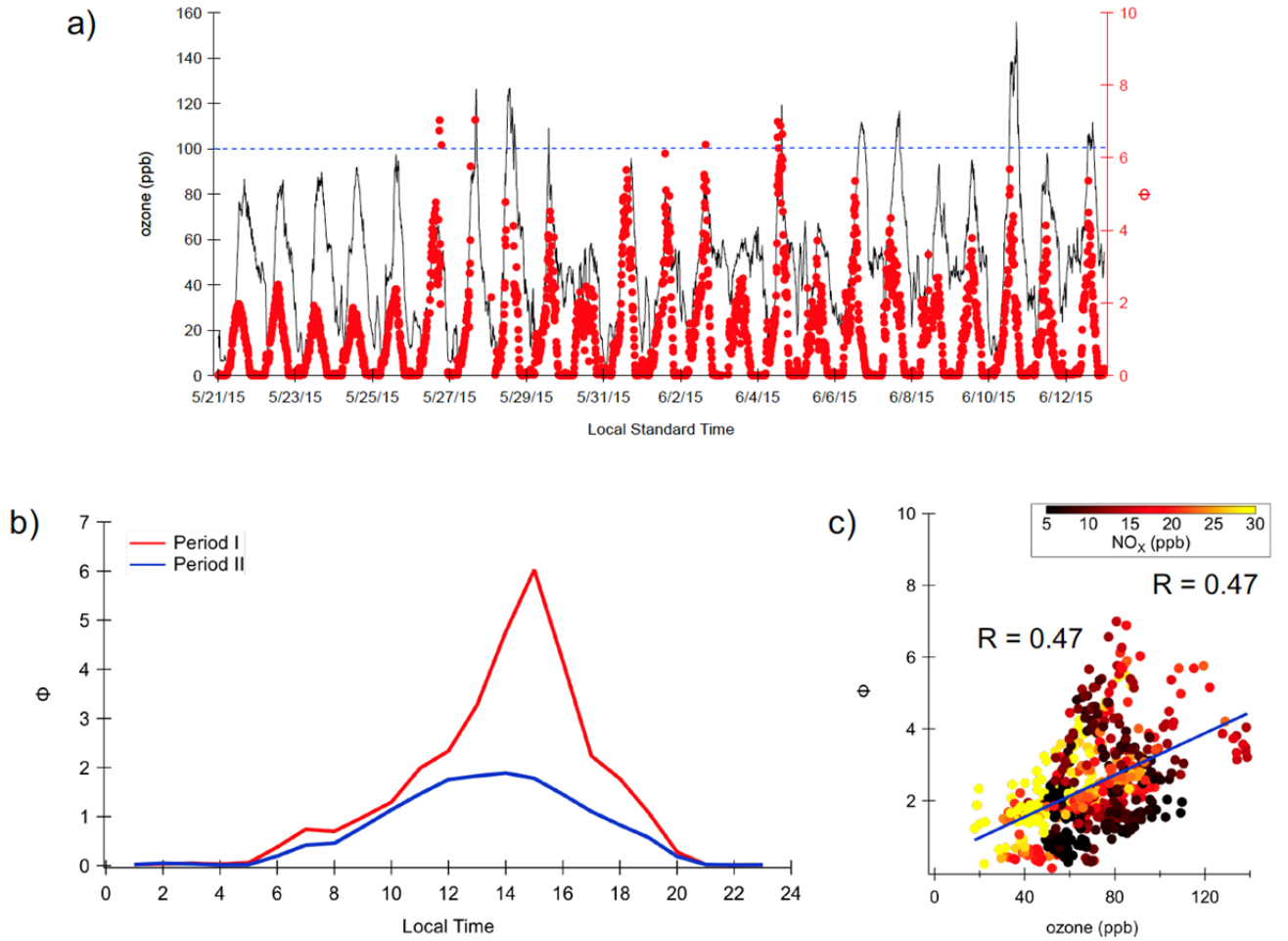

Fig. 5. (a) Temporal variation of ozone and the Leighton constant (Φ) during the MAPS-2015 Seoul field campaign. The dashed blue line shows ozone levels at 100 ppb (b) the diurnal variations of the Leighton constant (Φ) for Period I (red) and Period II (blue), and (c) correlation between the Leighton constant (Φ) and ozone for the time between 13:00 and 15:00 local standard time. Each data point is color coded by NO_x mixing ratios.

uncertainty, there are some distinctive differences between Periods I and II. First, higher levels of OH reactivity were observed in the afternoon (~33%) during Period I compared to Period II. The criteria pollutants (CO, NO_x, O_3, and SO_2) contributed to 70% of the calculated OH reactivity during Period II and 61% during Period I. In contrast, the VOC contribution to the calculated OH reactivity is assessed much higher during Period I (39%) then that (30%) of Period II as shown in one data point at 4 p.m. local time in Fig. 6. Regardless of these differences, the relative contributions from the VOC class to OH reactivity have a similar distribution (Fig. 7). In both cases, BVOCs, mostly isoprene, contribute the most to the VOC reactivity. There are some noticeable differences in contributions to calculated OH reactivity from aromatics and OVOCs in two periods. The differences are collectively evaluated in a box model simulation exercise presented below. In addition, a detailed description on VOC speciation observed during the campaign can be found in Kim *et al.* (2016).

Kim *et al.* (2016) also presented a regional model (a nested GEOS-Chem framework) that estimated OH reactivity. In general, the model simulated OH reactivity was significantly lower than observed (~30%). NO_x and VOCs were estimated to contribute to 34% and 55% of the total OH reactivity, respectively, resembling the relative contributions in Period I. We ran multiple box-model simulations to evaluate ozone production potential of three different air mixtures—Period I, Preiod II, and the regional model products. The simulation results are presented in Fig. 8. As expected, the air mixture from Period I produces more ozone during the three-hour time scale (Fig. 8(a)). The time evolution of ozone from the model simulation of the GEOS-Chem simulated air mixture followed the pattern of the air mixture simulation for Period I, but with a smaller increment. This makes sense as relative contributions to OH reactivity from NO_x and VOCs are similar for both air mixtures. However, the total trace gas reactivity is assessed to be smaller in the air mixture simulated by GEOS-Chem. On the other hand, the simulated ozone temporal evolution for the air mixture of Period II indicates a different pattern—steady state is quickly achieved with rapid initial ozone production. These differences can be examined further with the simulated net ozone production rates illustrated in Fig. 8(b). The Period II air mixture shows a

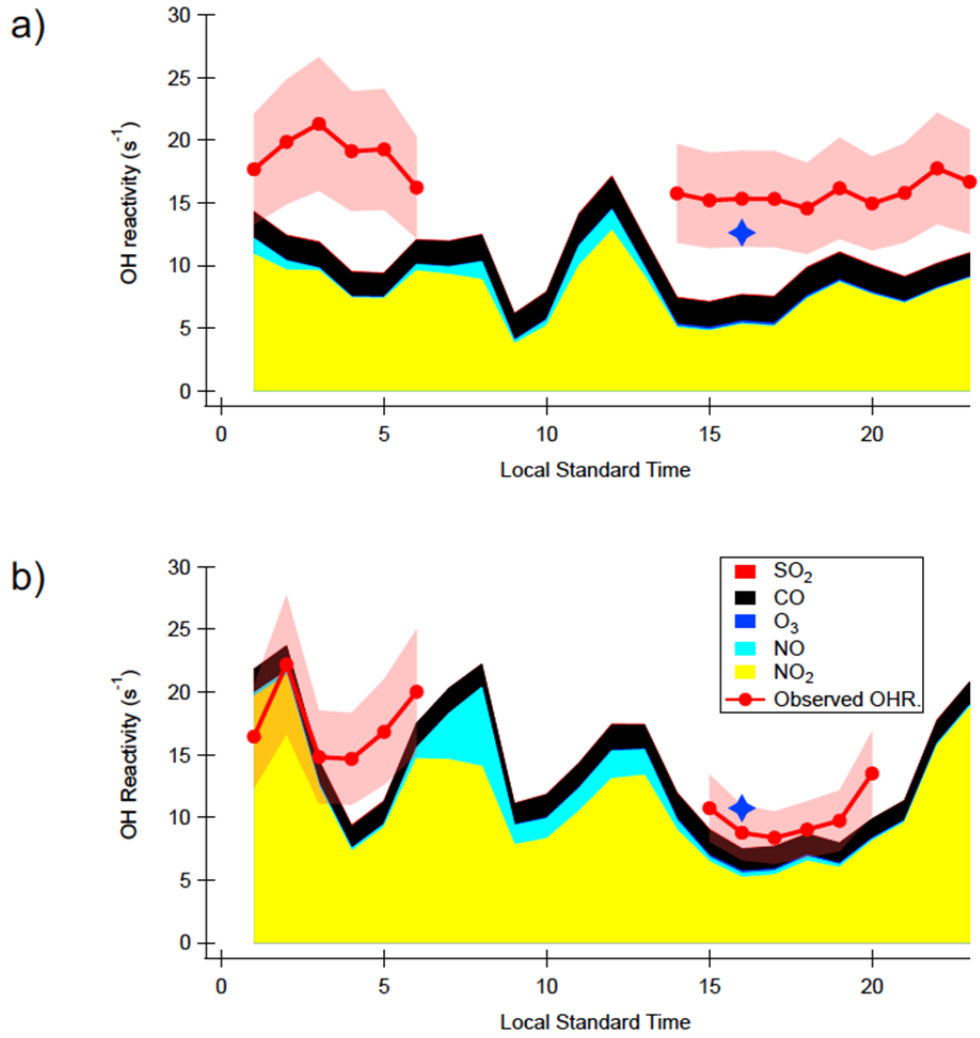

Fig. 6. The diurnal averages of observed and calculated OH reactivity during (a) Period I and (b) Period II. The Blue starts notate calculated OH reactivity including OH reactivity calculated from the VOC observations, conducted 4 pm at the local time.

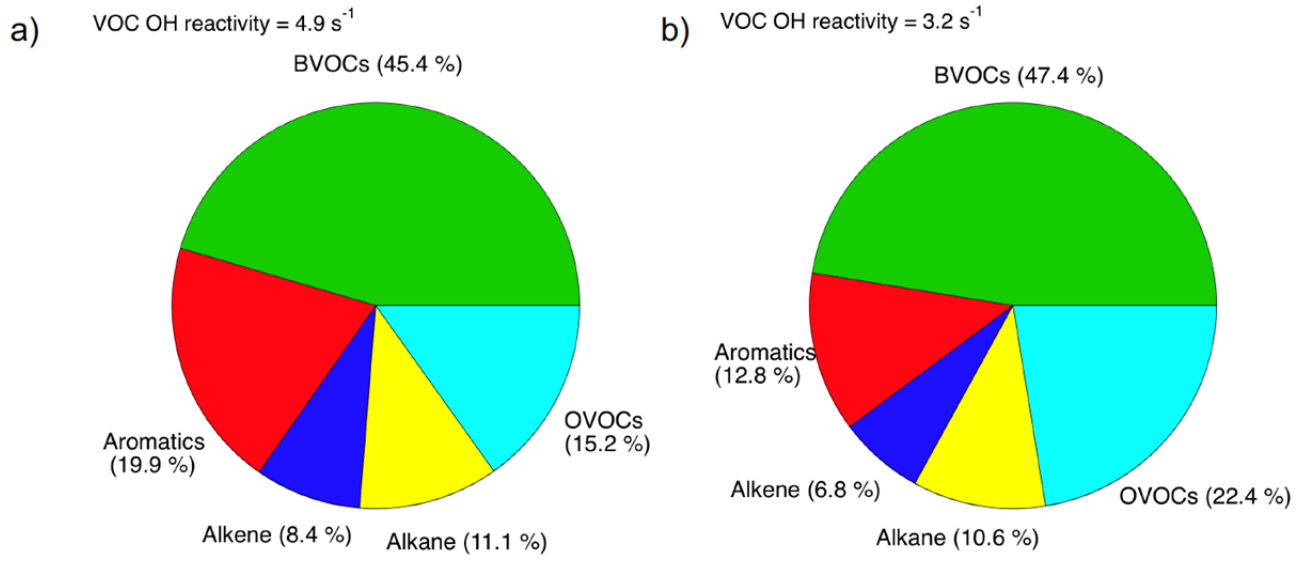

Fig. 7. OH reactivity contributions from different classes of VOCs for (a) Period I and (b) Period II (OVOCs notate oxygenated VOCs).

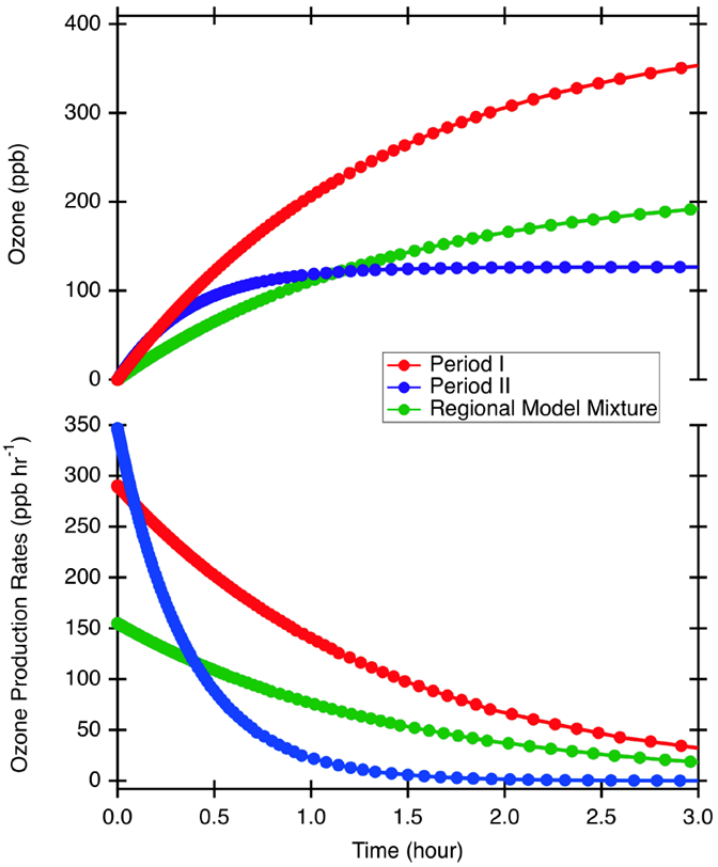

Fig. 8. Box model simulations of (a) ozone production and (b) net ozone production rates using different air mixtures. A detailed description of the different model scenarios is found in the text.

rapid initial net ozone production followed by a rapid decrease in ozone production. However, the mixtures of Period I and the regional model simulation illustrate more sustained net ozone production rates. The outcomes reflect different roles of NO_x and VOCs in photochemistry. In the beginning of Period II, the relatively high contribution of NO_2 to OH reactivity generates more ozone but the role of peroxy radicals from VOC oxidation become more important in ozone production as time progresses. Therefore, the model simulations with more relative contributions from VOCs to their calculated OH reactivity suggest there is more sustained ozone production under these scenarios. These modeling exercises clearly demonstrate the importance of considering the relative contributions of NO_x and VOCs to OH reactivity in order to assess ozone production potential.

SUMMARY AND CONCLUSION

We examined the photochemistry of high ozone episodes in Seoul, South Korea, during the MAPS campaign of spring 2015. The Leighton constant was consistently assessed at higher levels (> 4) during the active photochemistry period (1–5 p.m. local time) compared to days with lower ozone concentrations under similar physical conditions, e.g., in terms of temperature and solar radiation. The comparisons of OH reactivity between higher and lower ozone episodes illustrate that the high ozone episode is associated with higher observed OH reactivity. Moreover, during this period, the contribution from VOCs to the OH reactivity is higher than that from NO_x. Indeed, the box model simulation results clearly indicate higher ozone production for the air mixture with higher OH reactivity and higher VOC contributions to that reactivity, which is consistent with ambient ozone observations. A previous study (Kim *et al.*, 2016) shows that a regional model underestimates the OH reactivity but slightly overestimates the relative contribution from VOCs to OH reactivity. The box model simulation with this air mixture results in ozone production behaviors that substantially differ from those in the observationally constrained box model outcomes, which highlights the importance of improving model performance for the proper diagnosis and prediction of regional ozone production and transport. Overall, this observationally constrained analysis demonstrates that VOCs are a limiting factor in ozone production in SMA. Consequently, the proposed NO_x-abatement policy may increase ozone production in the beginning as the sustained influence of BVOCs is uncontrollable (Carlton *et al.*, 2010); however, policy makers should not hesitate to implement this plan. Rather, this study urges aggressive NO_x abatement in order to significantly reduce ozone production. The reduction in NO_x will also help to reduce tropospheric oxidation capacity, which positively correlates secondary aerosol production (Palm *et al.*, 2018).

ACKNOWLEDGEMENTS

This research was supported by National Institute of Environmental Research of Ministry of Environment in South Korea. The authors would like to express our sincere gratitude to KIST providing the experimental site.

REFERENCES

Blacet, F.E. (1952). Photochemistry in the lower atmosphere. *Ind. Eng. Chem.* 44: 1339–1342.

Calvert, J.G. (1976). Test of theory of ozone generation in Los-Angeles atmosphere. *Environ. Sci. Technol.* 10: 248–256.

Carlton, A.G., Pinder, R.W., Bhave, P.V. and Pouliot, G.A. (2010). To what extent can biogenic SOA be controlled? *Environ. Sci. Technol.* 44: 3376–3380.

Colman, J.J., Swanson, A.L., Meinardi, S., Sive, B.C., Blake, D.R. and Rowland, F.S. (2001). Description of the analysis of a wide range of volatile organic compounds in whole air samples collected during PEM-tropics A and B. *Anal. Chem.* 73: 3723–3731.

Crawford, J., Davis, D., Chen, G., Bradshaw, J., Sandholm, S., Gregory, G., Sachse, G., Anderson, B., Collins, J., Blake, D., Singh, H., Heikes, B., Talbot, R. and Rodriguez, J. (1996). Photostationary state analysis of the NO_2-NO system based on airborne observations from the western and central North Pacific. *J. Geophys. Res.* 101: 2053–2072.

Griffin, R.J., Beckman, P.J., Talbot, R.W., Sive, B.C. and Varner, R.K. (2007). Deviations from ozone photostationary state during the International Consortium for Atmospheric Research on Transport and Transformation 2004 campaign: Use of measurements and photochemical modeling to assess potential causes. *J. Geophys. Res.* 112: D10S07.

Haagen-Smit, A.J. (1952). Chemistry and physiology of Los Angeles smog. *Ind. Eng. Chem.* 44: 1342–1346.

Jenkin, M.E., Young, J.C. and Rickard, A.R. (2015). The MCM v3.3.1 degradation scheme for isoprene. *Atmos. Chem. Phys.* 15: 11433–11459.

Kim, S., Lee, M., Kim, S., Choi, S., Seok, S. and Kim, S. (2013). Photochemical characteristics of high and low ozone episodes observed in the Taehwa Forest observatory (TFO) in June 2011 near Seoul South Korea. *Asia-Pac. J. Atmos. Sci.* 49: 325–331.

Kim, S., Kim, S.Y., Lee, M., Shim, H., Wolfe, G.M., Guenther, A.B., He, A., Hong, Y. and Han, J. (2015). Impact of isoprene and HONO chemistry on ozone and OVOC formation in a semirural South Korean forest. *Atmos. Chem. Phys.* 15: 4357–4371.

Kim, S., Sanchez, D., Wang, M., Seco, R., Jeong, D., Hughes, S., Barletta, B., Blake, D.R., Jung, J., Kim, D., Lee, G., Lee, M., Ahn, J., Lee, S.D., Cho, G., Sung, M.Y., Lee, Y.H., Kim, D.B., Kim, Y., Woo, J.H., Jo, D., Park, R., Park, J.H., Hong, Y.D. and Hong, J.H. (2016). OH reactivity in urban and suburban regions in Seoul, South Korea - An East Asian megacity in a rapid transition. *Faraday Discuss.* 189: 231–251.

Kirchner, F., Jeanneret, F., Clappier, A., Kruger, B., van den Bergh, H. and Calpini, B. (2001). Total VOC reactivity in the planetary boundary layer: 2. A new indicator for determining the sensitivity of the ozone production to VOC and NO_x. *J. Geophys. Res.* 106: 3095–3110.

Lee, G., Ahn, J.Y., Jang, I.S., Park, J.H. and Hong, Y. (2017). The extensive ground measurements of air quality during the KORUS-AQ/MAPS-Seoul 2016, AOGS, 2017, Singapore.

Levy, H. (1971). Normal atmosphere - Large radical and formaldehyde concentrations predicted. *Science* 173: 141–143.

Palm, B.B., de Sa, S.S., Day, D.A., Campuzano-Jost, P., Hu, W.W., Seco, R., Sjostedt, S.J., Park, J.H., Guenther, A.B., Kim, S., Brito, J., Wurm, F., Artaxo, P., Thalman, R., Wang, J., Yee, L.D., Wernis, R., Isaacman-VanWertz, G., Goldstein, A.H., Liu, Y.J., Springston, S.R., Souza, R., Newburn, M.K., Alexander, M.L., Martin, S.T. and Jimenez, J.L. (2018). Secondary organic aerosol formation from ambient air in an oxidation flow reactor in central Amazonia. *Atmos. Chem. Phys.* 18: 467–493.

Parrish, D.D., Trainer, M., Williams, E.J., Fahey, D.W., Hubler, G., Eubank, C.S., Liu, S.C., Murphy, P.C., Albritton, D.L. and Fehsenfeld, F.C. (1986). Measurements of the NO_x-O_3 photostationary state at Niwot Ridge, Colorado. *J. Geophys. Res.* 91: 5361–5370.

Ridley, B.A., Madronich, S., Chatfield, R.B., Walega, J.G., Shetter, R.E., Carroll, M.A. and Montzka, D.D. (1992). Measurements and model simulations of the photostationary state during the Mauna Loa Observatory Photochemistry Experiment: Implications for radical concentrations and ozone production and loss rates. *J. Geophys. Res.* 97: 10375–10388.

Sanchez, D., Jeong, D., Seco, R., Wrangham, I., Park, J.H., Brune, W.H., Koss, A., Gilman, J., de Gouw, J., Misztal, P., Goldstein, A., Baumann, K., Wennberg, P.O., Keutsch, F.N., Guenther, A. and Kim, S. (2018). Intercomparison of OH and OH reactivity measurements in a high isoprene and low NO environment during the Southern Oxidant and Aerosol Study (SOAS). *Atmos. Environ.* 174: 227–236.

Seinfeld, J.H. (1989). Urban air-pollution - State of the science. *Science* 243: 745–752.

Sinha, V., Williams, J., Diesch, J.M., Drewnick, F., Martinez, M., Harder, H., Regelin, E., Kubistin, D., Bozem, H., Hosaynali-Beygi, Z., Fischer, H., Andres-Hernandez, M.D., Kartal, D., Adame, J.A. and Lelieveld, J. (2012). Constraints on instantaneous ozone production rates and regimes during DOMINO derived using in-situ OH reactivity measurements. *Atmos. Chem. Phys.* 12: 7269–7283.

Wolfe, G.M., Marvin, M.R., Roberts, S.J., Travis, K.R. and Liao, J. (2016). The framework for 0-D Atmospheric Modeling (F0am) V3.1. *Geosci. Model Dev.* 9: 3309–3319.

Received for review, November 1, 2017
Revised, April 17, 2018
Accepted, June 16, 2018